

Fast sound in binary fluid mixtures

A. Campa* and E. G. D. Cohen

The Rockefeller University, 1230 York Avenue, New York, New York 10021

(Received 6 December 1989)

The calculations and the results that predicted a fast-sound mode in low- as well as high-density binary fluid mixtures are presented in detail. Kinetic theory was used, which allowed a detailed discussion of the microscopic dynamics of the fluid in terms of eigenmodes. The Bhatnagar-Gross-Krook approximation method extended to binary mixtures was employed to solve the appropriate kinetic equation and to obtain approximate eigenmodes of the mixture. The fast-sound mode appears far beyond the hydrodynamic regime as either an extension to higher wave numbers of the hydrodynamic sound eigenmode or as a kinetic eigenmode. Some recent and possible future experiments are discussed.

I. INTRODUCTION

In three recent publications¹⁻³ the presence of an experimentally observable propagating mode, with a velocity considerably in excess of that of sound, was predicted for low- as well as high-density binary noble-gas-like fluid mixtures. This fast propagating mode was called fast sound as in the original work by Bosse *et al.*⁴ on the possible existence of such a mode in liquid $\text{Li}_{0.8}\text{Pb}_{0.2}$ alloys, suggested by computer simulations of these alloys. In these papers it was suggested that this fast propagating mode would appear far outside the hydrodynamic regime and would be associated with the dynamics of the light component only and would give a visible pronounced shoulder or peak in the partial dynamic structure factor $S_{11}(k, \omega)$ of the light component 1. No shoulder would appear in $S_{12}(k, \omega)$ and $S_{22}(k, \omega)$, where 2 refers to the heavy component of the mixture. This shoulder in $S_{11}(k, \omega)$ leads, for a proper choice of the two components, to a shoulder in $d^2\sigma/d\omega d\Omega$, the differential cross section for light or neutron scattering, which is proportional to a weighted average of the $S_{ij}(k, \omega)$ ($i, j=1, 2$). This new phenomenon is most pronounced in disparate mass mixtures, where the ratio of the mass of the light component to that of the heavy component is small. Since the characteristic length for low-density gases, the mean free path l , is the order of 10^{-5} cm, light scattering must be used to detect the fast mode in such mixtures. On the other hand, in dense mixtures the characteristic length is of the order of the size of the particles, i.e., 10^{-8} cm, so that neutron scattering must be used to detect the fast mode in this case. In addition, in light scattering experiments the polarizabilities of the molecules of the two components should be comparable, while in neutron scattering experiments the nuclear scattering lengths for neutrons should be comparable in order to have a distinguishable contribution from the light component to $d^2\sigma/d\omega d\Omega$ [cf. (2.7)]. Thus the possibility of detecting fast sound was predicted for dense He-Xe mixtures, where the mass ratio is $m_{\text{Xe}}/m_{\text{He}} \approx 33$ and the scattering length ratio $b_{\text{Xe}}/b_{\text{He}} \approx 1.49$ and low-

density H_2 -Ar mixtures, where the mass ratio is $m_{\text{Ar}}/m_{\text{H}_2} \approx 20$ and the polarizability ratio is $\alpha_{\text{Ar}}/\alpha_{\text{H}_2} \approx 2$. It was pointed out in Ref. 2, that even for mass ratios closer to 1, fast sound might still be observable. Montfrooij *et al.* confirmed this prediction by molecular dynamics⁵ as well as by neutron scattering⁶ for dense mixtures of 80% helium-20% neon. In addition, Wegdam *et al.*⁷ very recently observed a fast propagating mode in low-density H_2 -Ar mixtures by light scattering experiments, in agreement with Ref. 3.

The details of the calculations that led to the theoretical predictions in the three publications¹⁻³ mentioned above will be reported here. In addition, a few comments on the subsequently carried out experiments^{6,7} will be made. The theory is based on a hard-sphere model of the mixture, for which an approximate kinetic theory (the revised Enskog theory) is available at all densities, so that a detailed discussion of the dynamical processes in the fluid, in particular its (approximate) eigenmodes, can be made. The revised Enskog theory used here is a generalization by de Schepper of that for a simple hard-sphere fluid to binary fluid mixtures.⁸ The paper is organized as follows. In Sec. II we give the basic formulas of the theory. In Sec. III we present results for low-density mixtures, while Sec. IV contains results for dense mixtures. Section V discusses the main results of the paper, the recent experiments, and some possible future experiments as well as some open problems.

II. THE REVISED ENSKOG THEORY

A. N -particle time correlation functions

The quantities of interest here are the partial dynamic structure factors

$$S_{ij}(k, \omega) = \frac{1}{2\pi} \int_{-\infty}^{+\infty} dt e^{i\omega t} F_{ij}(k, t), \quad (2.1)$$

which are the time Fourier transforms of the partial intermediate scattering functions $F_{ij}(k, t)$. These are defined by

$$F_{ij}(k, t) = \langle \delta n_i^*(\mathbf{k}) e^{iL} \delta n_j(\mathbf{k}) \rangle_N. \quad (2.2)$$

Here \mathbf{k} is a wave vector with length $k = |\mathbf{k}| \neq 0$, the brackets $\langle \rangle_N$ indicate an equilibrium average over a canonical ensemble of N_1 particles of species 1, with mass m_1 and N_2 particles of species 2, with mass m_2 ($N = N_1 + N_2$), in a volume V at temperature T , with partial number densities $n_i = N_i/V$ ($i=1,2$); the asterisk denotes complex conjugation. The dynamical variable $\delta n_i(\mathbf{k})$ is (for $i=1,2$) the fluctuation of the number density of the i th component, which for $k \neq 0$ is given by

$$\delta n_i(\mathbf{k}) = \frac{1}{(N_i)^{1/2}} \sum_{p=1}^{N_i} e^{-i\mathbf{k} \cdot \mathbf{r}_p^{(i)}}, \quad (2.3)$$

where $\mathbf{r}_p^{(i)}$ is the position of particle p of species i . In (2.2) L is the pseudo-Liouville-operator for hard spheres,⁹ which, for binary mixtures, is given by

$$L = \sum_{i=1}^2 \sum_{p=1}^{N_i} \mathbf{v}_p^{(i)} \cdot \frac{\partial}{\partial \mathbf{r}_p^{(i)}} + \frac{1}{2} \sum_{i=1}^2 \sum_{j=1}^2 \sum_{p=1}^{N_i} \sum_{q=1}^{N_j} T_{pq}^{(i,j)}, \quad (2.4)$$

where $\mathbf{v}_p^{(i)}$ is the velocity of particle p of species i . The first term in (2.4) describes the free streaming, while the collision operator $T_{pq}^{(i,j)}$ describes a binary collision between particle p of species i and particle q of species j . $T_{pq}^{(i,j)}$ is given by

$$T_{pq}^{(i,j)} = \sigma_{ij}^2 \int d\hat{\sigma} \delta(\mathbf{r}_{pq}^{(i,j)} + \sigma^{(i,j)}) \times \Theta(\mathbf{v}_{pq}^{(i,j)} \cdot \hat{\sigma}) | \mathbf{v}_{pq}^{(i,j)} \cdot \hat{\sigma} | [b_{pq}^{(i,j)}(\hat{\sigma}) - 1]. \quad (2.5)$$

Here $\mathbf{r}_{pq}^{(i,j)} = \mathbf{r}_p^{(i)} - \mathbf{r}_q^{(j)}$, $\mathbf{v}_{pq}^{(i,j)} = \mathbf{v}_p^{(i)} - \mathbf{v}_q^{(j)}$; $\sigma^{(i,j)} = \sigma_{ij} \hat{\sigma}$, where $\sigma_{ij} = (\sigma_i + \sigma_j)/2$, with σ_i the hard-sphere diameter of particles of species i ; $\hat{\sigma}$ is a unit vector and $\Theta(x)$ is the Heaviside step function. The substitution operator $b_{pq}^{(i,j)}(\hat{\sigma})$ transforms the precollisional velocities into the postcollisional velocities

$$b_{pq}^{(i,j)}(\hat{\sigma}) \mathbf{v}_p^{(i)} = \mathbf{v}_p^{(i)'} = \mathbf{v}_p^{(i)} - 2 \frac{\mu_{ij}}{m_i} (\mathbf{v}_{pq}^{(i,j)} \cdot \hat{\sigma}) \hat{\sigma}, \quad (2.6)$$

$$b_{pq}^{(i,j)}(\hat{\sigma}) \mathbf{v}_q^{(j)} = \mathbf{v}_q^{(j)'} = \mathbf{v}_q^{(j)} + 2 \frac{\mu_{ij}}{m_j} (\mathbf{v}_{pq}^{(i,j)} \cdot \hat{\sigma}) \hat{\sigma},$$

with the reduced mass $\mu_{ij} = m_i m_j / (m_i + m_j)$. By definition, the operator $b_{pq}^{(i,j)}(\hat{\sigma})$, acting on any function of $\mathbf{v}_p^{(i)}$ and/or $\mathbf{v}_q^{(j)}$, transforms these velocities into those given by (2.6). In (2.4) we make the convention that $T_{pp}^{(i,i)} = 0$ (i.e., a particle does not collide with itself), and in addition we have that $T_{pq}^{(i,j)} = T_{qp}^{(j,i)}$. This follows from (2.5), when we use $b_{pq}^{(i,j)}(\hat{\sigma}) = b_{pq}^{(i,j)}(-\hat{\sigma}) = b_{qp}^{(j,i)}(\hat{\sigma})$, as can be checked in (2.6). The δ function and the step function in (2.5) assure, respectively, that the two particles collide only when they are at a distance σ_{ij} and are moving towards each other.

The $S_{ij}(k, \omega)$ in (2.1) and the $F_{ij}(k, t)$ in (2.2) depend only on k because of the isotropy of the equilibrium state. In classical fluids all the $S_{ij}(k, \omega)$ are real, even functions of ω , and symmetric in i and j : $S_{12}(k, \omega) = S_{21}(k, \omega)$. As mentioned before, the differential scattering cross section $d^2\sigma/d\omega d\Omega$ for light or neutron scattering is proportional to a weighted average of the $S_{ij}(k, \omega)$,

$$\frac{d^2\sigma}{d\omega d\Omega} \propto x_1 c_1^2 S_{11}(k, \omega) + x_2 c_2^2 S_{22}(k, \omega) + 2(x_1 x_2)^{1/2} c_1 c_2 S_{12}(k, \omega), \quad (2.7)$$

where $x_i = n_i / (n_1 + n_2)$ is the relative number concentration in the mixture of particles of species i . For light scattering $c_i = \alpha_i$, the polarizability of a particle of species i , while for neutron scattering $c_i = b_i$, the effective scattering length of a nucleus of species i .

B. One-particle expressions

The correlation functions $F_{ij}(k, t)$ in (2.2) can be computed approximately on the one-particle level using the revised Enskog theory.⁸ We first introduce a linear (real) space whose elements are two-component functions $\mathbf{f}(\mathbf{v}_1, \mathbf{v}_2)$:

$$\mathbf{f}(\mathbf{v}_1, \mathbf{v}_2) = \begin{bmatrix} f_1(\mathbf{v}_1) \\ f_2(\mathbf{v}_2) \end{bmatrix}, \quad (2.8)$$

where $f_1(\mathbf{v}_1)$ and $f_2(\mathbf{v}_2)$ are the components of the function $\mathbf{f}(\mathbf{v}_1, \mathbf{v}_2)$. In this space we introduce the average $\langle \langle \mathbf{f}(\mathbf{v}_1, \mathbf{v}_2) \rangle_1 \rangle_2$, defined by

$$\langle \langle \mathbf{f}(\mathbf{v}_1, \mathbf{v}_2) \rangle_1 \rangle_2 = \int d\mathbf{v}_1 d\mathbf{v}_2 \phi_0^{(1)}(\mathbf{v}_1) \phi_0^{(2)}(\mathbf{v}_2) \times [f_1(\mathbf{v}_1) + f_2(\mathbf{v}_2)], \quad (2.9)$$

where $\phi_0^{(i)}(\mathbf{v})$ is the Maxwell distribution for particles of species i ,

$$\phi_0^{(i)}(\mathbf{v}) = \left[\frac{\beta m_i}{2\pi} \right]^{3/2} e^{-\beta m_i v^2/2}, \quad (2.10)$$

with $\beta = 1/k_B T$, k_B being Boltzmann's constant. Our linear space becomes a (real) Hilbert space once we define the scalar product between two functions $\mathbf{f}(\mathbf{v}_1, \mathbf{v}_2)$ and $\mathbf{f}'(\mathbf{v}_1, \mathbf{v}_2)$ as

$$\langle \langle \mathbf{f}(\mathbf{v}_1, \mathbf{v}_2), \mathbf{f}'(\mathbf{v}_1, \mathbf{v}_2) \rangle_1 \rangle_2 = \int d\mathbf{v}_1 d\mathbf{v}_2 \phi_0^{(1)}(\mathbf{v}_1) \phi_0^{(2)}(\mathbf{v}_2) \times [f_1(\mathbf{v}_1) f_1'(\mathbf{v}_1) + f_2(\mathbf{v}_2) f_2'(\mathbf{v}_2)]. \quad (2.11)$$

This scalar product can also be interpreted as the average (2.9) for the product of the two functions $\mathbf{f}(\mathbf{v}_1, \mathbf{v}_2)$ and $\mathbf{f}'(\mathbf{v}_1, \mathbf{v}_2)$. Here the product of two functions is defined component by component, and is also obtained by the usual multiplication of the row (bra) $\langle \langle \mathbf{f}(\mathbf{v}_1, \mathbf{v}_2) |$ with the column (ket) $| \mathbf{f}'(\mathbf{v}_1, \mathbf{v}_2) \rangle_1 \rangle_2$.

Having made these definitions, the functions $F_{ij}(k, t)$ in (2.2) are approximated by $F_{ij}^E(k, t)$, which are obtained from (2.2) by going from the N -particle to the single-particle level and making the following replacements,^{2,8,10-12} the details of which can be found in Refs. 8 and 10: (i) The N -particle average $\langle \rangle_N$ is replaced by the average $\langle \langle \rangle_1 \rangle_2$. (ii) The N -particle pseudo-Liouville-operator is replaced by a single-particle kinetic operator $L_E(\mathbf{k})$, which depends parametrically on \mathbf{k} and acts on the Hilbert space of two-component functions $\mathbf{f}(\mathbf{v}_1, \mathbf{v}_2)$. (iii) The N -particle functions $\delta n_i(\mathbf{k})$ ($i=1,2$)

are replaced by two suitable two-component functions $\phi_1^{(i)}(\mathbf{v}_1, \mathbf{v}_2; k)$ ($i=1,2$), which depend parametrically on k . Then

$$F_{ij}(k, t) \approx F_{ij}^{E(k, t)} = \langle \langle \phi_1^{(i)}(\mathbf{v}_1, \mathbf{v}_2; k) e^{iL_E(\mathbf{k})} \phi_1^{(j)}(\mathbf{v}_1, \mathbf{v}_2; k) \rangle \rangle_1 \rangle_2. \quad (2.12)$$

The two functions $\phi_1^{(i)}(\mathbf{v}_1, \mathbf{v}_2; k)$ ($i=1,2$) we need are

$$\begin{aligned} \phi_1^{(1)}(\mathbf{v}_1, \mathbf{v}_2; k) &= \begin{bmatrix} [S_{11}(k)]^{1/2} \cos[\alpha(k)] \\ [S_{11}(k)]^{1/2} \sin[\alpha(k)] \end{bmatrix}, \\ \phi_1^{(2)}(\mathbf{v}_1, \mathbf{v}_2; k) &= \begin{bmatrix} [S_{22}(k)]^{1/2} \sin[\alpha(k)] \\ [S_{22}(k)]^{1/2} \cos[\alpha(k)] \end{bmatrix}, \end{aligned} \quad (2.13)$$

where

$$\alpha(k) = \frac{1}{2} \arcsin \frac{S_{12}(k)}{[S_{11}(k)S_{22}(k)]^{1/2}}, \quad (2.14)$$

We note that these $\phi_1^{(i)}$ are actually independent of $\mathbf{v}_1, \mathbf{v}_2$, but we keep the formal dependence on $\mathbf{v}_1, \mathbf{v}_2$ for the sake of mathematical generality. Here the $S_{ij}(k) = F_{ij}(k, 0)$ are the partial static structure factors of the mixture. The two functions $\phi_1^{(i)}(\mathbf{v}_1, \mathbf{v}_2; k)$ ($i=1,2$) are linear combinations of the two basic orthonormal functions [in the scalar product (2.11)],

$$\begin{aligned} \psi_1^{(1)}(\mathbf{v}_1, \mathbf{v}_2) &= \begin{bmatrix} \psi_1^{(1)}(\mathbf{v}_1) \\ 0 \end{bmatrix} = \begin{bmatrix} 1 \\ 0 \end{bmatrix}, \\ \psi_1^{(2)}(\mathbf{v}_1, \mathbf{v}_2) &= \begin{bmatrix} 0 \\ \psi_1^{(2)}(\mathbf{v}_2) \end{bmatrix} = \begin{bmatrix} 0 \\ 1 \end{bmatrix}, \end{aligned} \quad (2.15)$$

and are such that

$${}^{(1)}\Lambda^{(i,i)}h(\mathbf{v}_i) = \sum_{i'=1}^2 n_{i'} \chi_{ii'} \sigma_{ii'}^2 \int d\hat{\sigma} d\mathbf{v}_3^{(i')} \phi_0^{(i')}(\mathbf{v}_3^{(i')}) | \mathbf{v}_{i3}^{(i')} \cdot \hat{\sigma} | \Theta(\mathbf{v}_{i3}^{(i')} \cdot \hat{\sigma}) [b_{i3}^{(i')}(\hat{\sigma}) - 1] h(\mathbf{v}_i^{(i)}), \quad (2.21)$$

with $\chi_{ij} = g_{ij}(\sigma_{ij})$ the radial distribution function at contact, while for $i=j$ or $i \neq j$,

$${}^{(2)}\Lambda_{\mathbf{k}}^{(i,j)}h(\mathbf{v}_j) = (n_i n_j)^{1/2} \chi_{ij} \sigma_{ij}^2 \int d\hat{\sigma} d\mathbf{v}_3^{(j)} e^{-i\mathbf{k} \cdot \sigma_{ij}} \phi_0^{(j)}(\mathbf{v}_3^{(j)}) | \mathbf{v}_{i3}^{(j)} \cdot \hat{\sigma} | \Theta(\mathbf{v}_{i3}^{(j)} \cdot \hat{\sigma}) [b_{i3}^{(j)}(\hat{\sigma}) - 1] h(\mathbf{v}_3^{(j)}). \quad (2.22)$$

The superscripts (1) and (2) on the left of the Λ 's correspond to parts which are independent of \mathbf{k} or dependent on \mathbf{k} , respectively. The third term in (2.18) represents the mean field operators

$$A_{\mathbf{k}}^{(i,j)}h(\mathbf{v}_j) = \int d\mathbf{v}_j^{(j)} \phi_0^{(j)}(\mathbf{v}_j^{(j)}) [A^{(i,j)}(k) \psi_2^{(i)}(\mathbf{v}_i^{(i)}) \psi_1^{(j)}(\mathbf{v}_j^{(j)}) + A^{(j,i)}(k) \psi_1^{(i)}(\mathbf{v}_i^{(i)}) \psi_2^{(j)}(\mathbf{v}_j^{(j)})] h(\mathbf{v}_j^{(j)}). \quad (2.23)$$

In (2.23) we have

$$\begin{aligned} \psi_1^{(i)}(\mathbf{v}) &= 1, \\ \psi_2^{(i)}(\mathbf{v}) &= (\beta m_i)^{1/2} v_z \quad (i=1,2) \end{aligned} \quad (2.24)$$

and

$$A^{(i,j)}(k) = \delta_{ij} \frac{ik}{(\beta m_i)^{1/2}} + B^{(i,j)}(k), \quad (2.25)$$

$$\langle \langle \phi_1^{(i)}(\mathbf{v}_1, \mathbf{v}_2; k) \phi_1^{(j)}(\mathbf{v}_1, \mathbf{v}_2; k) \rangle \rangle_2 = S_{ij}(k), \quad (2.16)$$

The meaning of the subscript 1 in the functions in (2.13) and (2.15) will become clear in Sec. II C. The operator $L_E(\mathbf{k})$, acting on a general vector function $\mathbf{f}(\mathbf{v}_1, \mathbf{v}_2)$, transforms this function into $\mathbf{f}'(\mathbf{v}_1, \mathbf{v}_2) = L_E(\mathbf{k})\mathbf{f}(\mathbf{v}_1, \mathbf{v}_2)$ according to the following matrix relation:

$$\begin{bmatrix} f'_1(\mathbf{v}_1) \\ f'_2(\mathbf{v}_2) \end{bmatrix} = \begin{bmatrix} L_E^{(1,1)}(\mathbf{k}) & L_E^{(1,2)}(\mathbf{k}) \\ L_E^{(2,1)}(\mathbf{k}) & L_E^{(2,2)}(\mathbf{k}) \end{bmatrix} \begin{bmatrix} f_1(\mathbf{v}_1) \\ f_2(\mathbf{v}_2) \end{bmatrix}. \quad (2.17)$$

The 2×2 matrix nature of $L_E(\mathbf{k})$ applies of course only to the component indices i, j of $L_E^{(i,j)}(\mathbf{k})$; each operator $L_E^{(i,j)}(\mathbf{k})$, and thus also $L_E(\mathbf{k})$, if expressed as a matrix, is an $\infty \times \infty$ matrix. $L_E^{(i,j)}(\mathbf{k})$ acts on functions of \mathbf{v}_j and yields functions of \mathbf{v}_i . In the following we will take for convenience \mathbf{k} parallel to the z axis since $F_{ij}(k, t)$ and $S_{ij}(k, \omega)$ depend only on k . The four "elements" $L_E^{(i,j)}(\mathbf{k})$ in (2.17) of the kinetic operator $L_E(\mathbf{k})$ are given by^{8,10}

$$L_E^{(i,j)}(\mathbf{k}) = -ikv_{iz} \delta_{ij} + \bar{\Lambda}_{\mathbf{k}}^{(i,j)} + A_{\mathbf{k}}^{(i,j)}. \quad (2.18)$$

The first term in (2.18) represents free streaming. The second term contains the collision operators given by

$$\bar{\Lambda}_{\mathbf{k}}^{(i,j)}f(\mathbf{v}_j) = \Lambda_{\mathbf{k}}^{(i,j)}f(\mathbf{v}_j) - \int d\mathbf{v}_i \phi_0^{(i)}(\mathbf{v}_i) \Lambda_{\mathbf{k}}^{(i,j)}f(\mathbf{v}_j), \quad (2.19)$$

with, for $i=j$,

$$\Lambda_{\mathbf{k}}^{(i,i)} = {}^{(1)}\Lambda^{(i,i)} + {}^{(2)}\Lambda_{\mathbf{k}}^{(i,i)} \quad (i=1,2)$$

and for $i \neq j$,

$$\Lambda_{\mathbf{k}}^{(i,j)} = {}^{(2)}\Lambda_{\mathbf{k}}^{(i,j)}. \quad (2.20)$$

Here, for $i=j$,

with

$$\begin{aligned}
 B^{(1,1)}(k) &= -\frac{ik}{(\beta m_1)^{1/2}} \left[\frac{S_{22}(k)}{S_{11}(k)S_{22}(k) - S_{12}^2(k)} \right]^{1/2} \cos[\alpha(k)] , \\
 B^{(1,2)}(k) &= \frac{ik}{(\beta m_1)^{1/2}} \left[\frac{S_{22}(k)}{S_{11}(k)S_{22}(k) - S_{12}^2(k)} \right]^{1/2} \sin[\alpha(k)] , \\
 B^{(2,1)}(k) &= \frac{ik}{(\beta m_2)^{1/2}} \left[\frac{S_{11}(k)}{S_{11}(k)S_{22}(k) - S_{12}^2(k)} \right]^{1/2} \sin[\alpha(k)] , \\
 B^{(2,2)}(k) &= -\frac{ik}{(\beta m_2)^{1/2}} \left[\frac{S_{11}(k)}{S_{11}(k)S_{22}(k) - S_{12}^2(k)} \right]^{1/2} \cos[\alpha(k)] .
 \end{aligned} \tag{2.26}$$

We note that in (2.13), (2.14), and (2.26) $S_{11}(k)$ and $S_{22}(k)$ are positive and that the Schwarz inequality $S_{11}(k)S_{22}(k) - S_{12}^2(k) \geq 0$ holds.

C. The BGK method

The time dependence of the $F_{ij}^E(k, t)$ in (2.12), governed by the evolution operator $\exp[tL_E(\mathbf{k})]$, is evaluated here using the Bhatnagar-Gross-Krook (BGK) method. In the BGK method^{10,11,13} the operator $L_E(\mathbf{k})$ is first converted into an $\infty \times \infty$ matrix, using a complete set of functions, after which the Laplace transform of the evolution operator $\exp[tL_E(\mathbf{k})]$, i.e., the resolvent operator $[z - L_E(\mathbf{k})]^{-1}$, is inverted explicitly. Here we need a complete set of functions depending only on $v_1 = |\mathbf{v}_1|$, v_{1z} , $v_2 = |\mathbf{v}_2|$, and v_{2z} . Such a complete set is constructed in the following way.

The set of functions (2.15) is extended to an orthonormal set [in the scalar product (2.11)], which is complete for functions depending on v_1 , v_{1z} , v_2 , and v_{2z} . We first introduce the two reduced (dimensionless) velocities $\mathbf{c}_1 = (\beta m_1/2)^{1/2} \mathbf{v}_1$ and $\mathbf{c}_2 = (\beta m_2/2)^{1/2} \mathbf{v}_2$, and the functions

$$\begin{aligned}
 \psi_n^{(i)}(\mathbf{v}_i) &= \psi_{r,l}^{(i)}(\mathbf{v}_i) \\
 &= N_{r,l} c_i^l Y_l^{(0)}(c_{iz}/c_i) S_r^{(l+1/2)}(c_i^2) \\
 & \quad [i=1,2; n=(r,l)] . \tag{2.27}
 \end{aligned}$$

Here $c_i = |\mathbf{c}_i|$; n stands for the pair of indices r, l , where r and $l=0,1,2, \dots$; $Y_l^{(0)}(x)$ is the spherical harmonic $Y_l^{(m)}(x)$ with $m=0$; $S_r^{(l+1/2)}(x)$ is the Sonine polynomial of degree r and index $l+1/2$,

$$S_r^{(l+1/2)}(x) = \frac{1}{r!} x^{-l-1/2} e^x \left[\frac{\partial}{\partial x} \right]^r e^{-x} x^{r+l+1/2} , \tag{2.28}$$

and $N_{r,l}$ is a normalization constant

$$N_{r,l} = \pi^{3/4} [2\Gamma(r+1)/\Gamma(r+l+3/2)]^{1/2} , \tag{2.29}$$

with $\Gamma(x)$ the gamma function. Next we introduce the following two-component functions:

$$\begin{aligned}
 \psi_n^{(1)}(\mathbf{v}_1, \mathbf{v}_2) &= \begin{bmatrix} \psi_n^{(1)}(\mathbf{v}_1) \\ 0 \end{bmatrix} , \\
 \psi_n^{(2)}(\mathbf{v}_1, \mathbf{v}_2) &= \begin{bmatrix} 0 \\ \psi_n^{(2)}(\mathbf{v}_2) \end{bmatrix}
 \end{aligned} \tag{2.30}$$

for $n=1,2, \dots$. For $n=1$, i.e., $(r,l)=(0,0)$, we recover the two functions (2.15), while for $n=2$, i.e., $(r,l)=(0,1)$, we recover for the components of $\psi_2^{(i)}(\mathbf{v}_1, \mathbf{v}_2)$ ($i=1,2$) the two functions (2.24). The set (2.30) is orthonormal:

$$\begin{aligned}
 \langle \langle \psi_l^{(i)}(\mathbf{v}_1, \mathbf{v}_2), \psi_m^{(j)}(\mathbf{v}_1, \mathbf{v}_2) \rangle_1 \rangle_2 &= \delta_{ij} \delta_{lm} \\
 & \quad (i, j=1,2; l, m=1,2, \dots) . \tag{2.31}
 \end{aligned}$$

The operator $L_E(\mathbf{k})$ is now represented by the infinite matrix with elements

$$[L_E(\mathbf{k})]_{lm}^{(i,j)} = \langle \langle \psi_l^{(i)}(\mathbf{v}_1, \mathbf{v}_2), L_E(\mathbf{k}) \psi_m^{(j)}(\mathbf{v}_1, \mathbf{v}_2) \rangle_1 \rangle_2 . \tag{2.32}$$

In the BGK approximation of order M to $L_E(\mathbf{k})$ the free streaming and the mean-field terms are taken into account exactly. Of the collision operator $\bar{\Lambda}_k$, whose ‘‘elements’’ $\bar{\Lambda}_k^{(i,j)}$ are given by (2.19)–(2.22), the first $2M \times 2M$ block of its matrix representation is taken into account exactly; these $2M \times 2M$ matrix elements are

$$\begin{aligned}
 \Omega_{lm}^{(i,j)}(k) &= \langle \langle \psi_l^{(i)}(\mathbf{v}_1, \mathbf{v}_2), \bar{\Lambda}_k \psi_m^{(j)}(\mathbf{v}_1, \mathbf{v}_2) \rangle_1 \rangle_2 \\
 & \quad (i, j=1,2; l, m=1,2, \dots, M) , \tag{2.33}
 \end{aligned}$$

while all other matrix elements are set equal to zero, except for the diagonal elements with $l=m > M$ and $i=j$, which are all set equal to a constant $d(k)$, which is chosen to be

$$\begin{aligned}
 d(k) &= x_1 \langle \psi_{M+1}^{(1)}(\mathbf{v}_1) \bar{\Lambda}_k^{(1)} \psi_{M+1}^{(1)}(\mathbf{v}_1) \rangle_1 \\
 & \quad + x_2 \langle \psi_{M+1}^{(2)}(\mathbf{v}_2) \bar{\Lambda}_k^{(1)} \psi_{M+1}^{(2)}(\mathbf{v}_2) \rangle_2 . \tag{2.34}
 \end{aligned}$$

Here $\bar{\Lambda}_k^{(1)}$ is the single fluid collision operator,^{11,12} and the average $\langle \rangle_i$ is given by $\langle \rangle_i = \int d\mathbf{v}_i \phi_0^{(i)}(\mathbf{v}_i) (\dots)$. Then, in the BGK approximation of order M , we have

$$L_E(\mathbf{k}) = f(\mathbf{k}) + F(\mathbf{k}) , \tag{2.35}$$

where the elements of the operators $f(\mathbf{k})$ are given by

$$f^{(i,j)}(\mathbf{k}) = [-ikv_{iz} + d(k)] \delta_{ij} , \tag{2.36}$$

so that $f(\mathbf{k})$ is a multiplicative operator. $F(\mathbf{k})$ is a finite-dimensional $2M \times 2M$ matrix operator that acts on a general two-component function $\mathbf{h}(\mathbf{v}_1, \mathbf{v}_2)$ as

$$\begin{aligned}
F(\mathbf{k})\mathbf{h}(\mathbf{v}_1, \mathbf{v}_2) &= \sum_{i=1}^2 \sum_{l=1}^M \sum_{j=1}^2 \sum_{m=1}^M |\psi_l^{(i)}(\mathbf{v}_1, \mathbf{v}_2)\rangle_1 \rangle_2 H_{lm}^{(i,j)}(k) \\
&\quad \times \langle \psi_m^{(j)}(\mathbf{v}_1, \mathbf{v}_2), \mathbf{h}(\mathbf{v}_1, \mathbf{v}_2) \rangle_1 \rangle_2
\end{aligned} \tag{2.37}$$

with

$$\begin{aligned}
H_{lm}^{(i,j)}(k) &= \langle \langle \psi_l^{(i)}(\mathbf{v}_1, \mathbf{v}_2), (\bar{A}_k + A_k) \psi_m^{(j)}(\mathbf{v}_1, \mathbf{v}_2) \rangle_1 \rangle_2 \\
&\quad - d(k) \delta_{im} \delta_{ij} \\
&\quad (i, j = 1, 2; l, m = 1, 2, \dots, M) .
\end{aligned} \tag{2.38}$$

Here the term $-d(k)\delta_{im}\delta_{ij}$ was obtained by first adding $d(k)$ to the diagonal matrix elements with $l, m \leq M$ and $i = j$ [and combining this with the other diagonal elements to obtain (2.36)], and then subtracting it, as shown in the last term of (2.38).

We now use the BGK approximation for L_E to compute the partial structure factors $S_{ij}(k, \omega)$. We consider

first the functions

$$\bar{F}_{lm}^{(i,j)E}(k, t) = \langle \langle \psi_l^{(i)}(\mathbf{v}_1, \mathbf{v}_2) e^{iL_E(\mathbf{k})t} \psi_m^{(j)}(\mathbf{v}_1, \mathbf{v}_2) \rangle_1 \rangle_2 , \tag{2.39}$$

and their Laplace transforms

$$\begin{aligned}
\tilde{S}_{lm}^{(i,j)E}(k, z) &= \int_0^\infty dt e^{-zt} \bar{F}_{lm}^{(i,j)E}(k, t) \\
&= \left\langle \left\langle \psi_l^{(i)}(\mathbf{v}_1, \mathbf{v}_2) \frac{1}{z - L_E(\mathbf{k})} \psi_m^{(j)}(\mathbf{v}_1, \mathbf{v}_2) \right\rangle_1 \right\rangle_2 .
\end{aligned} \tag{2.40}$$

The functions (2.40) are the ones actually computed by inverting the operator $z - L_E(\mathbf{k})$ with the BGK method, as will be shown in the next paragraph. Then, from the $\tilde{S}_{11}^{(i,j)E}(k, z)$ one can compute the partial dynamic structure factors $S_{ij}(k, \omega)$, given in (2.1). In fact, if we write

$$S_{11}^{(i,j)E}(k, \omega) = \frac{1}{\pi} \text{Re} \tilde{S}_{11}^{(i,j)E}(k, i\omega) , \tag{2.41}$$

we have from (2.13) for our kinetic approximation to the partial dynamic structure factors

$$\begin{aligned}
S_{11}(k, \omega) &= S_{11}(k) \{ S_{11}^{(1,1)E}(k, \omega) \cos^2[\alpha(k)] + S_{11}^{(2,2)E}(k, \omega) \sin^2[\alpha(k)] + 2S_{11}^{(1,2)E}(k, \omega) \sin[\alpha(k)] \cos[\alpha(k)] \} , \\
S_{22}(k, \omega) &= S_{22}(k) \{ S_{11}^{(1,1)E}(k, \omega) \sin^2[\alpha(k)] + S_{11}^{(2,2)E}(k, \omega) \cos^2[\alpha(k)] + 2S_{11}^{(1,2)E}(k, \omega) \sin[\alpha(k)] \cos[\alpha(k)] \} , \\
S_{12}(k, \omega) &= S_{21}(k, \omega) = [S_{11}(k) S_{22}(k)]^{1/2} \{ [S_{11}^{(1,1)E}(k, \omega) + S_{11}^{(2,2)E}(k, \omega)] \cos[\alpha(k)] \sin[\alpha(k)] + S_{11}^{(1,2)E}(k, \omega) \} .
\end{aligned} \tag{2.42}$$

In the BGK approximation of order M the inversion of the operator $z - L_E(\mathbf{k})$ is accomplished in the following way. With $L_E(\mathbf{k})$ given by (2.35), we use the operator identity

$$\frac{1}{z - [f(\mathbf{k}) + F(\mathbf{k})]} = \frac{1}{z - f(\mathbf{k})} + \frac{1}{z - f(\mathbf{k})} F(\mathbf{k}) \frac{1}{z - [f(\mathbf{k}) + F(\mathbf{k})]} \tag{2.43}$$

to get, for $l, m \leq M$ and $i, j = 1, 2$,

$$\tilde{S}_{lm}^{(i,j)E}(k, z) = \left[\frac{1}{I - A(k, z)H(k)} A(k, z) \right]_{lm}^{(i,j)} . \tag{2.44}$$

In the $2M \times 2M$ matrix on the right-hand side of (2.44), we have the $2M \times 2M$ unit matrix I , the $2M \times 2M$ matrix $H(k)$, with elements $H_{lm}^{(i,j)}(k)$ given by (2.38) and the $2M \times 2M$ matrix $A(k, z)$, with elements

$$\begin{aligned}
A_{lm}^{(i,j)}(k, z) &= \delta_{ij} \left\langle \left\langle \psi_l^{(i)}(\mathbf{v}_1, \mathbf{v}_2) \frac{1}{z + ikv_{iz} - d(k)} \psi_m^{(j)}(\mathbf{v}_1, \mathbf{v}_2) \right\rangle_1 \right\rangle_2 \\
&\quad (i, j = 1, 2; l, m = 1, 2, \dots, M) .
\end{aligned} \tag{2.45}$$

D. Discrete BGK eigenvalues

Alternatively, it is also possible to evaluate the functions $\tilde{S}_{lm}^{(i,j)E}(k, z)$ in terms of the eigenmodes of $L_E(\mathbf{k})$ with discrete eigenvalues. These eigenvalues are associated with the poles of the resolvent operator $[z - L_E(\mathbf{k})]^{-1}$, viz., with the $2M$ values $z = z_n(k)$ ($n = 1, 2, \dots, 2M$) which satisfy the equation^{10,11,13}

$$D(k, z) = \det[I - A(k, z)H(k)] = 0 . \tag{2.46}$$

Then, the ‘‘exact’’ expression (2.44) is replaced by

$$\tilde{S}_{lm}^{(i,j)E}(k, z) = \sum_{n=1}^{2M} \frac{M_{lm,n}^{(i,j)}(k)}{z - z_n(k)} , \tag{2.47}$$

where the $z_n(k)$ are the discrete eigenvalues of $L_E(\mathbf{k})$ and the $M_{lm,n}^{(i,j)}(k)$ are the corresponding amplitudes, given by

$$M_{lm,n}^{(i,j)}(k) = \frac{1}{D'(k, z_n(k))} [G(k, z_n(k)) A(k, z_n(k))]_{lm}^{(i,j)} , \tag{2.48}$$

where G is the transpose of the matrix of cofactors of $I - AH$ and

$$D'(k, z_n(k)) = \left. \frac{\partial D(k, z)}{\partial z} \right|_{z=z_n(k)} . \tag{2.49}$$

The difference between (2.44) and (2.47) is that in (2.47)

the essential singularity of $\tilde{S}_{lm}^{(i,j)E}(k,z)$ for $\text{Re}z = -\infty$ has been neglected.

The eigenvalues can be divided into real and complex eigenvalues. All eigenvalues have negative real parts.¹³ The complex eigenvalues come in complex conjugate pairs. The complex eigenvalues describe propagation; their real part represents the damping, while their imaginary part represents the propagation. Two complex conjugate eigenvalues represent propagation in opposite directions. The real eigenvalues represent purely damped (diffusive) processes. As will be seen later, in all the cases studied in this paper, the computation of the density-density correlation functions using only the discrete eigenvalues gives results which are indistinguishable from those given by the "exact" expression, the matrix inversion formula (2.44). Therefore the dynamical processes that determine the $S_{ij}(k,\omega)$ can be understood in terms of the eigenmodes with discrete eigenvalues of $L_E(\mathbf{k})$ only. In the following we will use the term propagating (eigen)mode to denote the two oppositely propagating (eigen)modes together.

The description in terms of discrete modes is a generalization of Landau-Placzek's theory of light scattering of fluids in terms of hydrodynamic modes,¹⁴ in that it makes a connection between the macroscopic properties of the fluid, as expressed by the $S_{ij}(k,\omega)$, and the microscopic properties of the fluid, as expressed by the modes obtained from a kinetic representation of the $L_E(\mathbf{k})$. Of all the eigenvalues of $L_E(\mathbf{k})$, only four eigenvalues go to zero when k goes to zero. They reduce to the four hydrodynamic eigenvalues that can also be derived from the hydrodynamic equations for binary mixtures:

$$\begin{aligned} z_{1,2}(k) &= \pm ic_s k - \Gamma_E k^2, \\ z_3(k) &= -D_{1E} k^2, \\ z_4(k) &= -D_{2E} k^2. \end{aligned} \quad (2.50)$$

The first two eigenvalues describe sound propagation (in opposite directions parallel to \mathbf{k}), with c_s the adiabatic sound velocity, while the other two eigenvalues describe purely diffusive (nonpropagating) processes. The coefficients Γ_E (the sound damping), D_{1E} , and D_{2E} can be expressed in terms of the transport coefficients, viz., the diffusion coefficient, the thermal conductivity, and the thermal diffusion coefficient, as well as thermodynamic quantities of the mixture.¹⁵ In the Enskog theory, indicated by a subscript E , they are obtained explicitly in terms of the diameters and masses of the two components and the thermodynamic state of the mixture, characterized by three independent thermodynamic variables such as the pressure, temperature, and concentration of one of the components.¹⁶ The extensions of the hydrodynamic modes to larger values of k , as obtained by kinetic theory, are called extended hydrodynamic modes.

E. Evaluation

The expressions that have to be evaluated are (a) for the "exact" evaluation of the $S_{ij}(k,\omega)$, the expression (2.44) together with (2.38) and (2.45) for the matrix elements; (b) for the $S_{ij}(k,\omega)$ in terms of the eigenmodes

with discrete eigenvalues, besides (2.38) and (2.45), the expressions (2.47)–(2.49), after the computation of the discrete eigenvalues themselves from (2.46). All these calculations have been carried out by computer. The nontrivial parts in these computations have been the matrix elements of $H(k)$ in (2.38), of $A(k,z)$ in (2.45), and the solution of (2.46). In the matrix elements of $H(k)$, the nontrivial contributions from the collision operator $\bar{\Lambda}_k$ have been obtained using generating functions for the $\psi_l^{(i)}(\mathbf{v}_1, \mathbf{v}_2)$.¹⁰ The matrix elements of $A(k,z)$ have been determined using a method introduced in Ref. 17, while the solutions of (2.46) were found with a computer subroutine.

III. LOW-DENSITY MIXTURES

A. Light scattering and polarizabilities

In hard-sphere mixtures the only relevant variables are the reduced (dimensionless) partial number densities $n_i \sigma_i^3$ ($i=1,2$), since the temperature scales out. The reduced (total) number density $n^* = n_1 \sigma_1^3 + n_2 \sigma_2^3$ is for low-density (gas) mixtures of the order of 10^{-2} – 10^{-3} , while the mean free paths l_i ($i=1,2$) of the molecules of the two components given by

$$1/l_i = \sqrt{2} \pi n_j \sigma_i^2 + (1 + m_i/m_j)^{1/2} \pi n_j \sigma_{ij}^2 \quad (i \neq j = 1,2), \quad (3.1)$$

are of the order of 10^{-5} cm. The range of values of the wave vector k for which the fast mode is present is such that kl_1 and kl_2 are of the order 1, which is well outside the hydrodynamic regime, where $kl_i \ll 1$ ($i=1,2$). Thus the relevant wavelengths are in the range of visible light and the differential scattering cross section is given by (2.7), with $c_i = \alpha_i$. Since the fast-sound mode is expected to be most prominent in disparate binary mixtures, where $m_1 \ll m_2$, one would in general have $\alpha_1 \ll \alpha_2$, as is the case for noble gases, the most natural example for using a hard-sphere approximation for the interaction of the fluid particles. However, as follows from (2.7), if $\alpha_1 \ll \alpha_2$, the only significant contribution to $d^2\sigma/d\omega d\Omega$ will come from $S_{22}(k,\omega)$ (assuming that x_1 and x_2 are of the same order). Therefore in order to have a visible contribution of the fast mode to $S_{11}(k,\omega)$, and $d^2\sigma/d\omega d\Omega$, we have to look for binary mixtures, where $m_1 \ll m_2$ but $\alpha_1 \approx \alpha_2$.

We chose, as a model mixture for our study of dilute binary mixtures, a H_2 -Ar mixture. In this case we have $m_{\text{Ar}}/m_{\text{H}_2} \approx 20 \gg 1$ (in atomic units these two masses are $m_{\text{H}_2} = 2.002$ and $m_{\text{Ar}} = 39.944$), but the polarizability of Ar is only about twice as much as that of H_2 .¹⁸

The equivalent hard-sphere diameters that we took for our H_2 -Ar mixture are, respectively, $\sigma_{\text{H}_2} = \sigma_1 = 2.760 \text{ \AA}$ and $\sigma_{\text{Ar}} = \sigma_2 = 3.659 \text{ \AA}$. We note that the equivalent hard-sphere diameter σ_i ($i=1,2$) of a given molecule in the gas phase at a given temperature is usually chosen such that the experimental value of the second virial coefficient or the viscosity agrees with the corresponding theoretical value for hard spheres. The same values are then used for the mixture, with $\sigma_{12} = (\sigma_1 + \sigma_2)/2$.

We remark that for low-density mixtures the density is an irrelevant variable since it comes in only via the mean free paths l_1 and l_2 . For, when $n^* < 10^{-2}$ and $l_i \sim 10^{-5}$ cm, $kl_i = O(1)$, but $k\sigma_i \ll 1$ ($i=1,2$). Then the k dependence of the collision operators $\bar{\Lambda}_k^{(i,j)}$ can be neglected [cf. (2.22)] and the mean-field operators $A_k^{(i,j)}$ can be neglected altogether. This means that the kinetic operators $L_E^{(i,j)}(\mathbf{k})$ reduce to the corresponding operators in the Boltzmann approximation. In that approximation, the matrix elements of the collision operators are all inversely proportional to the mean free paths l_i , i.e., proportional to n^* [cf. (3.1)], so that the ratio of the matrix elements of the streaming terms ($\sim k$) to those of the collision terms is kl_i ($i=1,2$). From this follows that all properties, in particular the $S_{ij}(k, \omega)$ and the eigenvalues $z_n(k)$, have a simple scaling behavior with respect to the density, via the l_i . All this obtains at fixed concentrations x_1 and x_2 and allows a variation of kl_i not only via a variation of k through the scattering angle, but also through the density n . Therefore we will present results for one reduced density only, viz., $n^* = 0.005$, and we will only vary the concentrations of the two components.

B. Results for H₂-Ar mixtures

In Fig. 1 we show eight eigenvalues, obtained in the BGK approximation with $2M=10$, for the two relative concentrations $x_{H_2} = 0.6$ and 0.8 . These are the least damped eigenmodes, i.e., those with the smallest absolute value of their real parts. Figure 1 and the following figures should be interpreted as follows. On the horizontal axis k is given in the dimensionless combination $k\sigma_{12}$; on the vertical axis the real parts of the eigenvalues are plotted on the negative side of this axis, while the absolute values of their imaginary parts are plotted on the positive side. The eigenvalues are made dimensionless by multiplication with a characteristic mean free time t_E ,

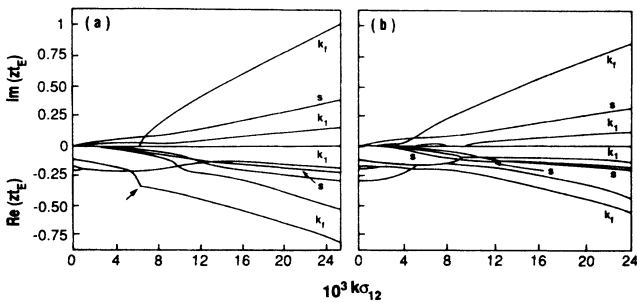


FIG. 1. Real part and absolute value of imaginary part of reduced eigenvalues of eight lowest eigenmodes for H₂-Ar mixture in the BGK approximation with $2M=10$ at $n^*=0.005$, (a) $x_{H_2}=0.6$, and (b) $x_{H_2}=0.8$, as a function of the reduced wave number. Labeling of eigenmodes is fast propagating kinetic mode = k_f ; (extended) sound mode = s ; slow propagating kinetic mode = k_1 ; no label = nonpropagating mode. In (a), k_f begins to propagate fast at $k\sigma_{12} = 0.006$, where two real eigenvalues, only one of which is shown, coalesce at arrow. In (b), a propagation gap in k_1 near $k\sigma_{12} \approx 0.009$ is clearly visible.

defined by

$$t_E = \frac{\sqrt{2\beta\mu}}{4\sqrt{\pi n \sigma_{12}^2 \chi_{12}}}, \quad (3.2)$$

where $\mu = m_1 m_2 / (m_1 + m_2)$ is the reduced mass and t_E reduces to the simple fluid mean free time¹³ when the two components are identical. Since complex eigenvalues come in complex conjugate pairs, each curve in the positive part of the vertical axis actually represents two eigenvalues, and so does the corresponding real part. At the value of k where two complex conjugate propagating eigenvalues appear (indicated by an arrow in Fig. 1), two real (nonpropagating) eigenvalues become equal.

We see in Fig. 1 that for both concentrations there is a fast kinetic mode, which propagates with a group velocity considerably greater than that of the (extended) sound mode. The eigenvalue corresponding to the fast propagating mode is indicated with k_f .

We will now discuss some of the details of the behavior of the eigenvalues as a function of $k\sigma_{12}$. In the case $x_{H_2} = 0.8$ we have a propagating kinetic mode which appears at $k\sigma_{12} \approx 0.0025$ and changes its slope markedly at $k\sigma_{12} \approx 0.005$, where it becomes a fast propagating mode. Its damping, for the values of k for which it propagates fast, is larger than that of the other modes. In the case $x_{H_2} = 0.6$ a propagating kinetic mode begins to propagate at about $k\sigma_{12} \approx 0.006$, and propagates fast immediately. Also in this case the damping of the fast propagating mode is larger than that of the other modes.

Because of these large dampings, it is not obvious to what extent the fast mode is important in the density-density correlation functions. We have computed the $S_{ij}(k, \omega)$ in the k range, where the eigenvalue associated with the fast mode has an imaginary part much larger (in absolute value) than those of the other complex eigenvalues. As an example we plot in Fig. 2 the $S_{ij}(k, \omega)$ and the differential scattering cross section $d^2\sigma/d\omega d\Omega$ for the case $x_{H_2} = 0.8$, for $k\sigma_{12} = 0.02$. The picture is similar for $x_{H_2} = 0.6$. We have used matrix inversion, as given by (2.44). In this and in the following figures, concerning the $S_{ij}(k, \omega)$ and $d^2\sigma/d\omega d\Omega$, we show only positive frequencies ω , since each $S_{ij}(k, \omega)$ is symmetric in ω ; also, the frequency ω is made dimensionless by multiplication with the mean free time t_E [cf. (3.2)], while the $S_{ij}(k, \omega)$

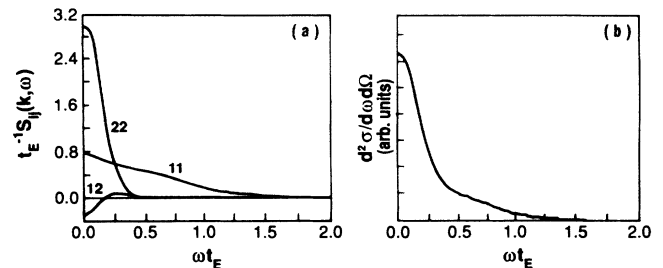


FIG. 2. (a) Reduced $S_{ij}(k, \omega)$ and (b) $d^2\sigma/d\omega d\Omega$ in arbitrary units for H₂-Ar mixture at $n^*=0.005$, $x_{H_2}=0.8$, and $k\sigma_{12}=0.02$, as a function of the reduced frequency. The curves in (a) are labeled by the corresponding ij values.

are made dimensionless by dividing by t_E . Since for the differential scattering cross section we neglect multiplicative factors [cf. (2.7)], we use arbitrary units in the corresponding figures for them. We see from Fig. 2 that the range of $S_{11}(k, \omega)$ in ω extends, with a pronounced shoulder, well beyond that of $S_{22}(k, \omega)$ and $S_{12}(k, \omega)$, and that the range of this shoulder is the same as that in which the fast mode occurs. This strongly suggests that the fast mode contributes only to $S_{11}(k, \omega)$. The shoulder in $S_{11}(k, \omega)$ is directly related to a shoulder in $d^2\sigma/d\omega d\Omega$, although this shoulder is much less pronounced.

To verify directly the contribution of the fast mode, we have computed again the $S_{ij}(k, \omega)$ using only the discrete eigenvalues. From (2.41), (2.42), and (2.47) it follows that in this approximation the $S_{ij}(k, \omega)$ are given by a sum of Lorentzians,

$$S_{ij}(k, \omega) = \frac{1}{\pi} \sum_n \operatorname{Re} \frac{A_{ij,n}(k)}{i\omega - z_n(k)}. \quad (3.3)$$

The $A_{ij,n}(k)$ are those combinations of the $M_{11,n}^{(i,j)}(k)$ obtained from (2.42) by replacing on the left-hand sides the $S_{ij}(k, \omega)$ by $A_{ij,n}(k)$ and on the right-hand sides the $S_{11}^{(i,j)E}(k)$ by $M_{11}^{(i,j)}(k)$. Using only the eight eigenvalues, plotted in Fig. 1(b), the $S_{ij}(k, \omega)$ are indistinguishable from those of Fig. 2. Therefore the contributions of the other two discrete eigenvalues and of the essential singularity (cf. Sec. II D) are negligible. Also, if we leave out the fast mode and compute the $S_{ij}(k, \omega)$ using only six discrete eigenvalues, $S_{12}(k, \omega)$ and $S_{22}(k, \omega)$ are indistinguishable from those of Fig. 2, while $S_{11}(k, \omega)$ and, consequently, $d^2\sigma/d\omega d\Omega$, change appreciably, in particular, in that their shoulders have disappeared. In Fig. 3 we show $S_{11}(k, \omega)$ and $d^2\sigma/d\omega d\Omega$ computed by matrix inversion (like in Fig. 2), and with six discrete eigenvalues. This is a direct demonstration that the fast mode contributes only to $S_{11}(k, \omega)$ and involves mainly the dynamics of the light component. This is also shown in Table I where the amplitudes corresponding to the eight eigenvalues used in the calculation of the $S_{ij}(k, \omega)$ are listed. From this table we can see that the dynamics of the two components appear to be approximately separated. In fact, the major contributions to A_{11} and A_{22} come from different sets of modes: from k_f and d_2 to A_{11} and from k_1 and d_1 to A_{22} . We note that the group velocity of the

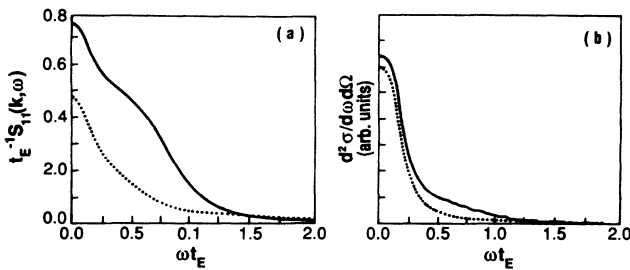


FIG. 3. (a) Reduced $S_{11}(k, \omega)$ and (b) $d^2\sigma/d\omega d\Omega$ in arbitrary units for H_2 -Ar mixture at $n^* = 0.005$, $x_{\text{H}_2} = 0.8$, and $k\sigma_{12} = 0.02$ as functions of the reduced frequency. The dotted lines are computed without the fast kinetic mode contribution.

fast mode is very close to the sound velocity in a corresponding pure H_2 fluid, i.e., a pure H_2 fluid, obtained by removing all the heavy particles from the mixture. The picture that we have just described concerning the $S_{ij}(k, \omega)$, holds for a broad range of relative concentrations, although the detailed behavior of the eigenvalues changes somewhat with concentration [cf. the differences between Figs. 1(a) and 1(b)].

We now turn to the problem of the range of concentrations for which a fast mode with an observable effect on $d^2\sigma/d\omega d\Omega$ is present. We have plotted, in Fig. 4, eight eigenvalues for the two concentrations $x_{\text{H}_2} = 0.3$ and 0.9 . We first discuss the latter [cf. Fig. 4(b)]. For $x_{\text{H}_2} = 0.9$, it is the extended sound mode, rather than a kinetic mode, that, for a value of $k\sigma_{12}$ around 0.005, increases its slope and begins to propagate fast. Correspondingly, the damping of the extended sound mode becomes larger than that of the other modes. In the region where this mode propagates faster than the other modes the group velocities of the extended sound mode is very close to the (ordinary) sound velocity of a pure low-density H_2 gas under similar conditions in analogy with previous cases. The difference in slope for the extended sound mode, between the hydrodynamic region ($k \rightarrow 0$) and the region where it propagates fast, is smaller than in the previous case because the difference between the sound velocity of

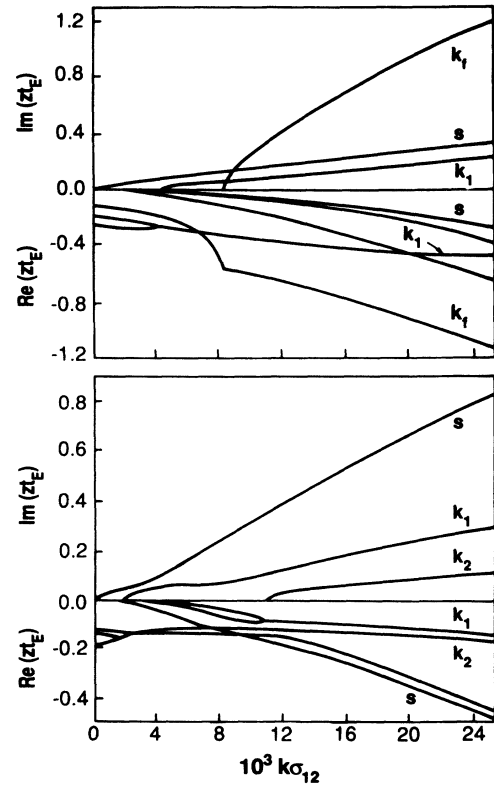


FIG. 4. Same as in Fig. 1 for (a) $x_{\text{H}_2} = 0.3$ and (b) $x_{\text{H}_2} = 0.9$. (a) Fast mode (k_f) is kinetic mode; k_1 is a slow propagating mode; (b) fast mode (s) is extended sound mode; k_1 and k_2 are propagating kinetic modes. As in Fig. 1, nonpropagating modes are not labeled.

TABLE I. Amplitudes at $k\sigma_{12}=0.02$ of the eight eigenvalues plotted in Fig. 1(b) for H_2 -Ar mixtures. k_f and k_1 are propagating kinetic modes, s is the sound mode; d_1 and d_2 are purely diffusive modes.

Mode	Eigenvalue	A_{11}	A_{22}	A_{12}
k_f	$-0.450 \pm 0.724i$	$0.254 \mp 0.254i$	$-6 \times 10^{-5} \pm 3 \times 10^{-4}i$	$-0.011 \mp 0.005i$
s	$-0.159 \pm 0.263i$	$-0.011 \pm 0.018i$	$-0.051 \mp 0.095i$	$0.048 \pm 7 \times 10^{-4}i$
k_1	$-0.124 \pm 0.094i$	$-0.008 \mp 0.006i$	$0.464 \mp 0.431i$	$0.004 \pm 0.082i$
d_1	-0.176	0.034	0.175	-0.077
d_2	-0.338	0.500	5×10^{-5}	-0.005

the pure H_2 gas and that of the H_2 -Ar mixture with $x_{H_2}=0.9$ decreases with increasing x_{H_2} , so that this difference will eventually disappear somewhere beyond $x_{H_2}=0.9$. We take $x_{H_2}=0.9$ as an upper limit for which a fast mode exists.

Next we turn to the case $x_{H_2}=0.3$. We see from Fig. 4(a) that the eigenvalues behave similarly as for $x_{H_2}=0.6$ [cf. Fig. 1(a)]: there is a kinetic fast mode that is fast as soon as it begins to propagate, and its group velocity is very close to the sound velocity of the corresponding pure H_2 gas. We now consider the $S_{ij}(k, \omega)$ for $x_{H_2}=0.3$ and $k\sigma_{12}=0.02$. They are plotted in Fig. 5. As in Fig. 2 matrix inversion and eight discrete eigenvalues give the same curves. However, there is no visible shoulder now in $S_{11}(k, \omega)$, only a very slow decrease of $S_{11}(k, \omega)$, which is practically not reflected in $d^2\sigma/d\omega d\Omega$ since x_{H_2} is smaller than in the previous cases so that the relative weight of $S_{11}(k, \omega)$ in $d^2\sigma/d\omega d\Omega$ is smaller. Therefore we take $x_{H_2} \approx 0.4$ as a lower limit for x_{H_2} , for an observable fast mode to be present.

C. Improved approximations

If we compute the $S_{ij}(k, \omega)$ for the k values of interest, where the fast mode is present, in the BGK approximation with $2M=20$ instead of $2M=10$, we find curves practically identical to those obtained with $2M=10$. In particular, the shoulder in $S_{11}(k, \omega)$ is unchanged. This gives some confidence that the $S_{ij}(k, \omega)$ have already reached their asymptotic dependence on M at $2M=10$ for these k values, so that they are stable with respect to an increase of the number M , when $2M \geq 10$.

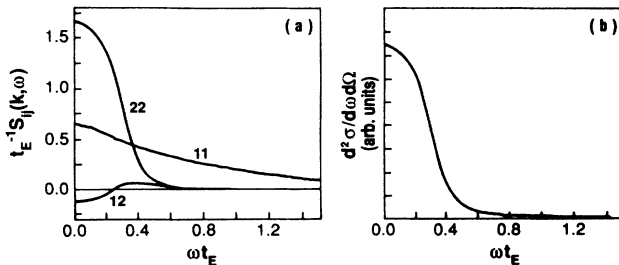


FIG. 5. Same as in Fig. 2 for $x_{H_2}=0.3$.

D. Experimental observability

As to experimental observation, the presence of the fast mode can be deduced from the presence of an extended shoulder in $d^2\sigma/d\omega d\Omega$. Although one can measure only $d^2\sigma/d\omega d\Omega$, and not the individual $S_{ij}(k, \omega)$, it is still possible to deduce that the fast mode contributes only to $S_{11}(k, \omega)$ in the following way. If we remove the H_2 molecules from the mixture and compute $d^2\sigma/d\omega d\Omega$ for the pure Ar fluid so obtained at the same k values as those of Figs. 2 and 3, we get a curve, shown in Fig. 6, which has a range practically identical to that of $S_{22}(k, \omega)$ in the mixture. This is consistent with what was observed earlier, viz., that the dynamics of the two components appear to be approximately separate. If one conjectures that the same would happen in a real mixture, then performing an experiment on pure Ar would give roughly the range of $S_{22}(k, \omega)$ in the H_2 -Ar mixture; if this range does not include the values for which $d^2\sigma/d\omega d\Omega$ has a shoulder, one could deduce that this shoulder must be due to $S_{11}(k, \omega)$. As far as $S_{12}(k, \omega)$ is concerned, we see that it is much smaller in absolute value than $S_{11}(k, \omega)$ and $S_{22}(k, \omega)$. This is to be expected since the integral of $S_{12}(k, \omega)$ over the frequency gives $S_{12}(k)$, the static cross structure factor, which is a small quantity at low densities, since it is then proportional to n^* . Finally, that the extended shoulder is due to a fast mode can be deduced also from the fact that its “center” is at a position, in ω , well above $\omega=c_s k$, where c_s is the velocity of sound of the mixture.

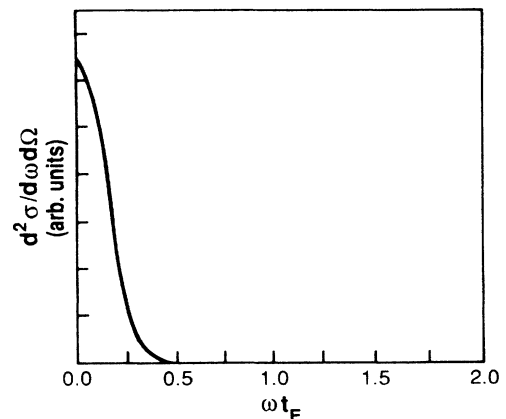


FIG. 6. $d^2\sigma/d\omega d\Omega$ in arbitrary units as a function of the reduced frequency for a pure Ar fluid obtained by removing the H_2 molecules from the mixture represented in Figs. 2 and 3.

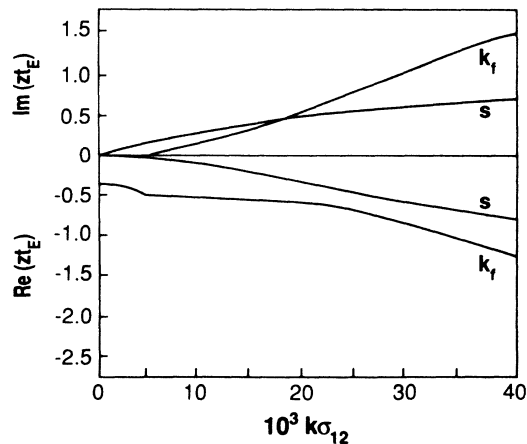


FIG. 7. Reduced eigenvalues of the fast kinetic sound mode (k_f) and the extended sound mode (s) are plotted for He-Ne mixtures as a function of the reduced frequency in the BGK approximation $2M = 10$ at $n^* = 0.005$ and $x_{\text{He}} = 0.6$.

E. Other mixtures

In this section we consider mixtures with a mass ratio closer to 1. We show that a fast mode is present also for these cases, although the effect is less dramatic.

As an example, in Fig. 7 we show the eigenvalues corresponding to the extended sound mode and to the fast mode, obtained with the BGK approximation $2M = 10$, for a He-Ne mixture. The reduced density is $n^* = 0.005$, and the relative concentration of the light component is 0.6. In atomic units the mass of He is 4.003, and the mass of Ne is 20.183 so that the mass ratio is about 5. Their (equivalent hard-sphere) diameters are taken to be $\sigma_{\text{He}} = 2.17 \text{ \AA}$ and $\sigma_{\text{Ne}} = 2.602 \text{ \AA}$, while for the polarizabilities we have $\alpha_{\text{Ne}} \approx 2\alpha_{\text{He}}$.

We see that a kinetic mode (k_f) begins to propagate faster at a certain value of k . Its group velocity is then very close to the velocity of sound of a pure low-density fluid obtained by removing the particles of the heavy component. Therefore still for a mass ratio around 5 a fast mode exists, although the difference in slopes between the fast mode and the sound mode is smaller than for larger mass ratios. In Fig. 8 we show the $S_{ij}(k, \omega)$ and the $d^2\sigma/d\omega d\Omega$ for He-Ne for $k\sigma_{12} = 0.04$. Now, as expected, the difference in range between $S_{11}(k, \omega)$ and

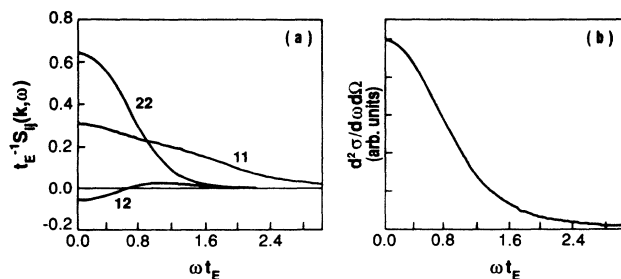


FIG. 8. (a) Reduced $S_{ij}(k, \omega)$ and (b) $d^2\sigma/d\omega d\Omega$ in arbitrary units as a function of the reduced frequency for He-Ne mixtures at $n^* = 0.005$, $x_{\text{He}} = 0.6$, and $k\sigma_{12} = 0.04$. Symbols as in Fig. 2.

$S_{22}(k, \omega)$ is smaller; moreover, the position of the shoulder in $S_{11}(k, \omega)$, attributed to the fast mode, is close to the position of the peak in $S_{12}(k, \omega)$, indicating that the fast mode also makes a sizeable contribution to $S_{12}(k, \omega)$. We will see that for higher densities the fast mode does not appear at all for hard-sphere mixtures with such small mass ratios.

IV. DENSE MIXTURES

A. Introduction

As mentioned before, for dense mixtures, where $n^* = n_1\sigma_1^3 + n_2\sigma_2^3$ is of the order 1, the relevant lengths are in the range of the wavelengths of thermal neutrons, so that the appropriate experiments are with neutron scattering. The differential scattering cross section is then given by (2.7) with $c_i = b_i$. For noble gases, the scattering lengths are all of the same order of magnitude, so that we do not have the problem of widely different scattering strengths as for the polarizabilities in the case of light scattering. In particular the scattering length of Xe is 1.488 that of He. We remark that with neutron scattering it is, in principle, possible to determine the $S_{ij}(k, \omega)$ separately.

For dense mixtures no simple scaling behavior with the density obtains, as at low densities, since the k dependence of the collision operator can now not be neglected. This k dependence is through $k\sigma_1$, $k\sigma_2$, and $k\sigma_{12}$ (cf. Sec. II), which are all of the order 1. Similarly, the mean-field operator is important at these densities.

In IV B we will present as an illustrative example results for dense He-Xe mixtures, for which extensive calculations have been carried out. The mass of Xe in atomic units is 131.30, so that the mass ratio $m_{\text{Xe}}/m_{\text{He}}$ is about 33. The diameters of He and Xe in a dense mixture are taken to be 2.21 and 3.91 \AA , respectively.

Since there is no good theory for the thermodynamic as well as the transport properties of dense gases or liquids, one chooses the equivalent hard-sphere diameters here in a different way than for dilute gases. In fact, one chooses them such that the first maximum in the static structure factors for the pure components at the given temperature of the mixture coincide with that of the corresponding hard-sphere fluids. The same values are then used for the mixture.

B. He-Xe mixtures

Like at low densities we found also at high densities that the dynamic structure factors $S_{ij}(k, \omega)$ are quite insensitive to an increase in the number M , the order of the BGK approximation when $2M \geq 10$. In Fig. 9 we plot the eigenvalues, corresponding to the propagating modes with the smallest damping, obtained in the BGK approximation with $2M = 16$, for mixtures with $n^* = 0.4$ and $x_{\text{He}} = 0.6$ and $x_{\text{He}} = 0.8$, respectively. The eigenmodes corresponding to 11 eigenvalues give, with (3.3), $S_{ij}(k, \omega)$ that are indistinguishable from those obtained by matrix inversion. We note the following: (a) For both relative concentrations there is a fast propagating kinetic mode.

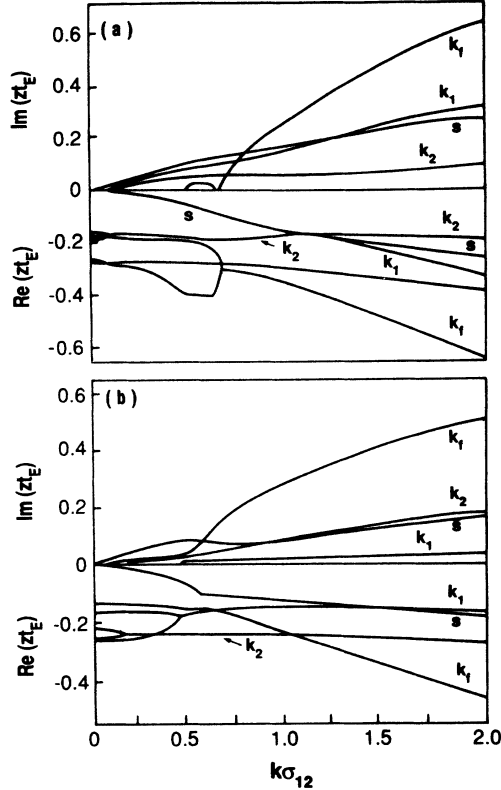


FIG. 9. Reduced eigenvalues, including the kinetic fast mode and the extended sound mode, are plotted as a function of the reduced wave number in the BGK approximation $2M=16$ for He-Xe mixtures at $n^*=0.4$, (a) $x_{\text{He}}=0.6$ and (b) $x_{\text{He}}=0.8$. Symbols as in Fig. 1; k_1 and k_2 are kinetic propagating modes. In Fig. 9(a), a propagation gap for the fast kinetic mode near $k\sigma_{12}\approx 0.75$ is clearly visible.

(b) For $x_{\text{He}}=0.8$ the fast mode is a kinetic mode that begins to propagate for a rather small value of $k\sigma_{12}$, and then starts to propagate faster at a value of $k\sigma_{12}$ around 0.6. (c) For $x_{\text{He}}=0.6$ the fast mode is a kinetic mode that begins to propagate fast immediately, for a value of $k\sigma_{12}$ around 0.65. (d) The group velocity of the fast mode is very close to the velocity of sound in the pure fluid obtained by removing all the heavy Xe atoms. (e) The fast mode always has the largest damping among all the plotted eigenvalues. However, like in low-density mixtures, this does not prevent a visible contribution of this mode to $S_{11}(k, \omega)$ and $d^2\sigma/d\omega d\Omega$ (cf. Fig. 10).

In Fig. 10 we plot the $S_{ij}(k, \omega)$ and the differential scattering cross section $d^2\sigma/d\omega d\Omega$ for the relative con-

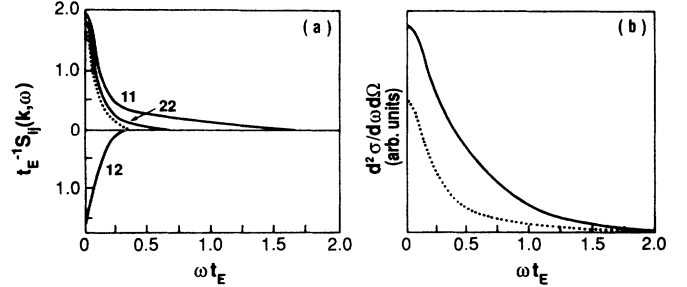


FIG. 10. (a) Reduced $S_{ij}(k, \omega)$ and (b) $d^2\sigma/d\omega d\Omega$ in arbitrary units as a function of the reduced frequency for He-Xe at $n^*=0.4$, $x_{\text{He}}=0.6$, and $k\sigma_{12}=1.8$. The dotted curves for $S_{11}(k, \omega)$ and $d^2\sigma/d\omega d\Omega$ are computed without the fast-sound mode contribution. Symbols as in Fig. 2.

centration $x_{\text{He}}=0.6$ and $k\sigma_{12}=1.8$. The shoulder in $S_{11}(k, \omega)$ is clearly visible. In the same figure we have also plotted $S_{11}(k, \omega)$ and $d^2\sigma/d\omega d\Omega$ obtained from the discrete eigenvalues of Fig. 9, except the fast mode. This does not affect $S_{12}(k, \omega)$ and $S_{22}(k, \omega)$, but it does affect $S_{11}(k, \omega)$. In Table II we show the amplitudes of the contributions of the various modes to the $S_{ij}(k, \omega)$, and we see that the fast mode only contributes to $S_{11}(k, \omega)$.

For other relative concentrations, we find that with an increasing concentration of He the fast mode tends to disappear. However, it is then the extended sound mode rather than a kinetic mode that has a sharp increase in its slope and will propagate fast, until at a concentration of $x_{\text{He}}\approx 0.9$ this sharp increase disappears. Thus we can take this value as the maximum concentration of He for fast sound to occur. With decreasing concentration of He the visible shoulder in $S_{11}(k, \omega)$ tends to disappear and only a very slow decrease in $S_{11}(k, \omega)$ with ω occurs, not reflected in $d^2\sigma/d\omega d\Omega$. This happens for concentrations somewhat lower than those for low-density mixtures, viz., at about $x_{\text{He}}=0.3$. Thus this is the lower limit of the He concentration for which fast sound can be observed in dense mixtures. As a function of density n^* we found that the fast mode tends to disappear with increasing density and, in fact, has disappeared for $n^*=0.8$.

C. Other mixtures

We briefly consider here other mixtures. We have found a fast propagating mode in He-Kr, where the mass ratio is about 21, but not in He-Ar, where the mass ratio is about 10. This in contrast to low-density mixtures, where we found a fast mode still for a mass ratio of about

TABLE II. Amplitudes at $k\sigma_{12}=1.8$ of the eight eigenvalues plotted in Fig. 9(a) for He-Xe mixtures. k_f , k_1 , and k_2 are propagating kinetic modes, s is the sound mode.

Mode	Eigenvalue	A_{11}	A_{22}	A_{12}
k_f	$-0.575 \pm 0.585i$	$0.220 \mp 0.253i$	$4 \times 10^{-4} \pm 3 \times 10^{-5}i$	$-0.005 \mp 0.011i$
s	$-0.243 \pm 0.257i$	$-0.035 \mp 0.007i$	$-0.025 \mp 0.047i$	$0.036 \pm 0.025i$
k_1	$-0.371 \pm 0.295i$	$0.001 \pm 6 \times 10^{-4}i$	$5 \times 10^{-4} \pm 0.001i$	$-9 \times 10^{-4} \pm 0.001i$
k_2	$-0.189 \pm 0.079i$	$-0.215 \mp 0.088i$	$-0.298 \mp 0.273i$	$0.258 \pm 0.164i$

5 (He-Ne mixtures). This seems to suggest that with increasing the density, a larger mass ratio is necessary to find fast sound in hard-sphere mixtures. This behavior differs from real mixtures in that Montfrooij *et al.*⁶ did find a fast propagating mode in He-Ne mixtures for a reduced density that in our hard-sphere model is estimated to be $n^* = 0.2$. In the following section we will discuss the reason for this difference.

V. DISCUSSION

The main subject of this paper has been the study of the characteristic behavior of disparate-mass binary fluid mixtures. In this class of fluids we find a new phenomenon far outside the hydrodynamic regime: one of the decay modes of the density fluctuations is a very fast propagating mode involving only the light component. This implies an effective separation of the dynamics of the light from the heavy particles. The presence of this fast propagating mode can be detected in light and neutron scattering experiments by a shoulder or peak in $S_{11}(k, \omega)$ as well as in $d^2\sigma/d\omega d\Omega$.

One can argue that the presence of a fast mode, which propagates only through the light particles, is due to the fact that its frequency is too high for the heavy particles to follow. However, the nature of the detailed physical mechanism that gives rise to this mode is not clear at present. In this connection it may be relevant that both at low and high densities, the group velocity associated with the fast mode has a value very close (about 1% difference) to the value of the sound velocity of the corresponding light particle fluid.

It is worthwhile to note that the mass ratio need not be very large in order to have an observable fast mode in dilute mixtures. On the other hand, in dense mixtures we found that, below a mass ratio of about 10, like in He-Ar, there is no fast mode anymore.

We found stability of the $S_{ij}(k, \omega)$ with respect to the change of the number M , which determines the order of the BGK approximation in our kinetic theory, as long as $M \geq 10$. This means that for a not very large value of M the corresponding approximate kinetic operator selects all the "effective" modes that are necessary to describe the dynamics of the density fluctuations.¹¹

We now want to argue why the fast mode causes a shoulder in $S(k, \omega)$ in spite of its large damping. To this end we will use the discrete eigenmodes of $L_E(\mathbf{k})$ and write a given eigenvalue (ignoring the subscript n and the dependence on k) as $z = i\omega_0 - \gamma$, where $\gamma > 0$ and is of the same order as $\omega_0 > 0$. Similarly, we write the corresponding amplitude $A = a + ib$. Then the corresponding Lorentzian contribution to $S(k, \omega)$ is given by

$$\text{Re} \frac{A + ib}{i(\omega - \omega_0) + \gamma} = \frac{a\gamma + b(\omega - \omega_0)}{(\omega - \omega_0)^2 + \gamma^2}. \quad (5.1)$$

The extrema of this curve are at the values

$$\omega = \omega_0 + \frac{\gamma}{b} [-a \pm (a^2 + b^2)^{1/2}]. \quad (5.2)$$

In the general case the various Lorentzians that compose the $S(k, \omega)$ overlap, so that they mix in a complicated manner and no contribution from any single one can be ascertained. However, for the fast mode ω_0 is well above the corresponding values of the other eigenvalues, and the equality $b = -a$ is approximately satisfied in all cases considered (cf. Tables I and II). Then the extrema of the corresponding Lorentzian are at

$$\omega = \omega_0 + \gamma(1 \pm \sqrt{2}), \quad (5.3)$$

where the smaller value is a maximum. Therefore we have a maximum at, approximately, $\omega \approx \omega_0 - 0.4\gamma$, which is reasonably displaced from the origin $\omega = 0$ and from the maxima of the other modes if their imaginary parts are well below ω_0 . This explains why we are able to see a shoulder corresponding to the fast mode, and why this shoulder is generally somewhat displaced towards the origin $\omega = 0$ with respect to the value $\omega = \omega_0$.

To the extent that the eigenmodes of the hard-sphere fluid correspond to those of a real fluid, the experimental observation of the fast mode in H₂-Ar (Ref. 7) and He-Ne (Ref. 6) mixtures implies that for the first time a nonhydrodynamic mode can be evidenced via the spectrum of the density fluctuations. In addition, they provide information on the extent of the validity of the hard-sphere approximation for real binary mixtures. In fact, the neutron scattering experiment on dense He-Ne mixtures⁶ shows that in real mixtures the damping of the fast mode is smaller than in hard-sphere mixtures, resulting in a peak or shoulder in $S_{11}(k, \omega)$ and $d^2\sigma/d\omega d\Omega$, where none was predicted by the hard-sphere model.

The experiments of Wegdam *et al.*⁷ appear to be consistent with a separation of the dynamics of the two components of the mixture. It is interesting to note that for values of $kl_i \approx 1.87$ a Gaussian behavior is found. This behavior appears in simple hard-sphere fluids only for the higher values $kl \geq 3$, where l is the mean free path in the simple fluid.¹¹

A number of open problems that deserve further investigation are the following. Since a fast mode has been found both for dilute and dense fluid mixtures, one could wonder whether such a mode would not also exist in disparate-mass solid mixtures. One would then have fast phonons propagating via the light component with a velocity greater than the velocity of sound of the solid mixture. A preliminary model calculation of a damped phonon propagation¹⁹ in solid mixtures would indicate that the above conjecture has some ground.

The physical situation of forced sound propagation in fluids due to an external macroscopic driving force is different from that of (fast) sound propagation due to internal microscopic density fluctuations, although the modes follow in both cases from the same dispersion relation $F(k, \omega) = 0$.¹ In fact, both types of modes are obtained by looking for plane-wave solutions of hydrodynamic or kinetic equations; for forced modes one solves then the dispersion relation for k in terms of a real ω , while for the study of (fast) sound one solves for eigenmodes, i.e., for ω in terms of a real k . The precise con-

nection between these two type of modes is unclear.

Finally, a more complete discussion of the behavior of the various eigenvalues as a function of k would be interesting. Looking at Fig. 1, we see that the slowest propagating mode has a propagation gap at $k\sigma_{12} \approx 0.009$, similar to propagating gaps found in simple hard-sphere fluids^{11,13} at values of $k\sigma$ close to where $S(k)$ has a maximum. It would be interesting to investigate the relevance of this phenomenon in more detail in binary mixtures and its possible connection with the behavior of

the static structure factors at the corresponding k values. This could then suggest a relation between the spatial ordering of the particles and the trapping of sound, which gives rise to these propagation gaps.²⁰

ACKNOWLEDGMENTS

This work was carried out in part under Grant No. DE-FG02-88-13847 of the U.S. Department of Energy.

*Present address: Dipartimento di Fisica, Università "La Sapienza," Piazzale Aldo Moro 2, 00185, Roma, Italy.

¹A. Campa and E. G. D. Cohen, in *Kinetic Theory and Extended Thermodynamics*, edited by I. Müller and T. Ruggeri (Pitagora, Bologna, Italy, 1987), p. 79.

²A. Campa and E. G. D. Cohen, *Phys. Rev. Lett.* **61**, 853 (1988).

³A. Campa and E. G. D. Cohen, *Phys. Rev. A* **39**, 4909 (1989).

⁴J. Bosse, G. Jacucci, M. Ronchetti, and W. Schirmacher, *Phys. Rev. Lett.* **57**, 3277 (1986).

⁵W. Montfrooij, P. Westerhuijs, and I. M. de Schepper, *Phys. Rev. Lett.* **61**, 2155 (1989).

⁶W. Montfrooij, P. Westerhuijs, V. O. de Haan, and I. M. de Schepper, *Phys. Rev. Lett.* **63**, 544 (1989).

⁷G. H. Wegdam, A. Bot, R. P. C. Schram, and H. M. Schaink, *Phys. Rev. Lett.* **63**, 2697 (1989).

⁸I. M. de Schepper and W. Montfrooij, *Phys. Rev. A* **39**, 5807 (1989).

⁹M. H. Ernst, J. R. Dorfman, W. R. Hoegy, and J. M. J. van Leeuwen, *Physica (Utrecht)* **45**, 127 (1969).

¹⁰A. Campa, Ph.D. thesis, The Rockefeller University, 1989.

¹¹B. Kamgar-Parsi, E. G. D. Cohen, and I. M. de Schepper,

Phys. Rev. A **35**, 4781 (1987).

¹²I. M. de Schepper and E. G. D. Cohen, *J. Stat. Phys.* **46**, 349 (1987).

¹³I. M. de Schepper and E. G. D. Cohen, *J. Stat. Phys.* **27**, 233 (1982).

¹⁴J. P. Boon and S. Yip, *Molecular Hydrodynamics* (MacGraw-Hill, New York, 1980).

¹⁵C. Cohen, J. W. H. Sutherland, and J. M. Deutch, *Phys. Chem. Liq.* **2**, 213 (1971).

¹⁶M. Lopez de Haro, E. G. D. Cohen, and J. M. Kincaid, *J. Chem. Phys.* **78**, 2746 (1983); J. M. Kincaid, M. Lopez de Haro, and E. G. D. Cohen, *ibid.* **79**, 4509 (1983); J. M. Kincaid, E. G. D. Cohen, and M. Lopez de Haro, *ibid.* **86**, 963 (1987).

¹⁷I. M. de Schepper, E. G. D. Cohen, and B. Kamgar-Parsi, *J. Stat. Phys.* **54**, 273 (1989).

¹⁸For nonspherical molecules like H₂, the polarizability is actually a tensor; we take here for the polarizability the average of the principal values of this tensor.

¹⁹A. Campa (unpublished).

²⁰T. R. Kirkpatrick, *Phys. Rev. A* **32**, 3130 (1985).